Sulfur-Doped Graphene with Iron Pyrite (FeS_2) as an Efficient and Stable Electrocatalyst for the Iodine Reduction Reaction in Dye-Sensitized Solar Cells

WILEY-VCH

DOI: 10.1002/((please add manuscript number))
Article type: Rapid Research Letter

Sulfur–Doped Graphene with Iron Pyrite (FeS_2) as an Efficient and Stable Electrocatalyst for the Iodine Reduction Reaction in Dye–sensitized Solar Cells

*Munkhbayar Batmunkh, Aabhash Shrestha, Gao Guo, Leping Yu, Jing Zhao, Mark. J. Biggs, Cameron J. Shearer and Joseph G. Shapter**

Munkhbayar Batmunkh, Dr. Aabhash Shrestha, Prof. Mark J. Biggs
School of Chemical Engineering, The University of Adelaide, Adelaide, South Australia 5005, Australia

Munkhbayar Batmunkh, Leping Yu, Dr. Jing Zhao, Dr. Cameron J. Shearer, Prof. Joseph G. Shapter
Centre for Nanoscale Science and Technology, School of Chemical and Physical Sciences, Flinders University, Bedford Park, Adelaide, South Australia 5042, Australia
E-mail: joe.shapter@flinders.edu.au

Prof. Gao Guo
Institute of Nano Biomedicine and Engineering, Shanghai Engineering Research Center for Intelligent Diagnosis and Treatment Instrument, Department of Instrument Science and Engineering, School of Electronic Information and Electrical Engineering, Shanghai Jiao Tong University, 800 Dongchuan Road, Shanghai 200240, P. R. China

Prof. Mark J. Biggs
School of Science, Loughborough University, Loughborough, Leicestershire, LE11 3TU, UK

Keywords: counter electrode, dye-sensitized solar cells, doping, graphene, iron disulfide

As an alternative to platinum (Pt), hybrid electrocatalysts based on sulfur–doped graphene with FeS_2 microspheres (SGN–FeS_2) were used as a counter electrode (CE) in dye–sensitized solar cells (DSSCs). Benefiting from the high conductivity of SGN and excellent electrocatalytic activity of the FeS_2, the bifunctional hybrid electrocatalyst based device displays a power conversion efficiency (PCE) of 8.1%, which is comparable to that (8.3%) of traditional Pt CE based DSSC, while also exhibiting excellent stability in ambient conditions. These characteristics, in addition to its low-cost and facile preparation, make the SGN–FeS_2 hybrid an ideal CE material for DSSCs.

Dye–sensitized solar cells (DSSCs) have attracted tremendous interest from the photovoltaic (PV) community owing to the potential they offer in terms of low manufacturing cost, high power conversion efficiency (PCE), and excellent stability.[1, 2] A typical DSSC consists of organic dye–sensitizers adsorbed onto a porous TiO_2 photoelectrode, an iodide/triiodide (I^-/I_3^-) redox electrolyte and a platinum (Pt) coated counter electrode (CE).[3] In this device structure, the Pt coated CE serves an essential role in reducing I_3^- to I^- (called the iodine reduction reaction, IRR). However, Pt is an expensive and relatively rare material, which limits its use in the large–scale commercialization of DSSCs.[4]

Over the past two decades, the development of alternative electrocatalysts that are low–cost and can exhibit higher or comparable performance to the conventional Pt has been the subject of intense research.[5, 6] The ideal CE materials for DSSCs should possess not only high electrical conductivity, but also excellent catalytic activity and stability.[7] A wide range of alternative materials have been explored as electrocatalysts for IRR in DSSCs.[7-13] Graphene nanosheets doped with heteroatoms such as sulfur (S),[14] nitrogen (N),[15] boron (B),[16] phosphorous (P)[17] show great promise as the catalyst for the IRR in DSSCs owing to their high surface area and good conductivity. Among the different doping atoms, S–doped graphene (SGN) has to date yielded the most efficient electrocatalyst for IRR (also found in our preliminary investigation, see supporting information (SI)).[14, 18] This is in part due to the sulfur "S" atoms being efficient electrocatalytic active sites for the IRR.[19] This good performance is also linked to the SGN possessing enhanced electrical conductivity and improved surface area compared to un-doped graphene,[20, 21] which helps improve the charge transfer process in DSSCs. Despite these advantages, the performance of devices fabricated with SGN only based CEs are still lower than that of the Pt based CEs cells because the electrocatalytic activity of single SGN for IRR is inferior to that of Pt.

Recently, iron pyrite (FeS_2), a narrow band–gap semiconductor, has been shown to be a promising candidate for use as a CE material in DSSCs owing to its abundance in nature, non–toxicity, low–cost as well as outstanding electrocatalytic activity.[22-24] Although FeS_2 has shown some promise as a CE material in DSSCs, its relatively low conductivity limits the further improvement of the device performances. Therefore combining the excellent catalytic activity of FeS_2 with the high conductivity of SGN would be a promising strategy to produce highly efficient electrocatalyst material for DSSC.

In this work, we report the preparation of Pt–free hybrid electrocatalysts, consisting of SGN nanosheets wrapped FeS_2, for use as CE materials in DSSCs. The DSSC device fabricated

with this hybrid electrocatalyst yields a PCE of 8.1%, which was comparable to that (8.3%) of the cell using Pt. Electrochemical measurements in combination with electrical conductivity analysis reveal that this remarkable PV performance of DSSC originates from the synergistic effect of this hybrid electrocatalyst, in which FeS_2 provides excellent electrocatalytic activity for the IRR, while SGN facilitates the electron–transfer process (**Scheme 1**).

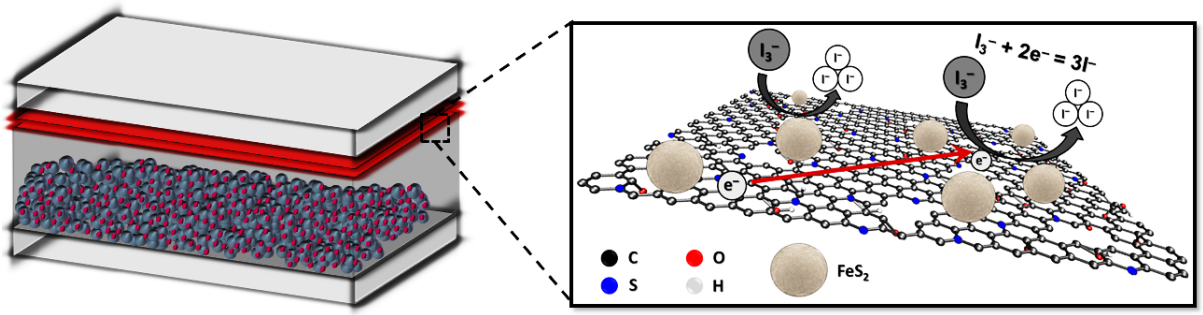

Scheme 1. Schematic illustration of DSSC device fabricated with SGN–FeS_2 electrocatalyst as a CE material. Note: FeS_2 spheres used in this scheme are from the scanning electron microscopy (SEM) images of the synthesized FeS_2.

In order to compare the doping effect of different heteroatoms on graphene in terms of their ability to catalyze the IRR in DSSC system, five individual nonmetallic elements (I, P, B, N, S) were selected and species containing each element were used to prepare single atom–doped GN materials. All the doped GN materials including I–doped GN (IGN), P–doped GN (PGN), B–doped GN (BGN), N–doped GN (NGN) and S–doped GN (SGN) were prepared from graphene oxide (GO) by using different precursors under the same experimental conditions (details can be found in the SI, Table S1). These heteroatom–doped graphene electrocatalysts were then used as CE materials in DSSCs. For comparison, DSSCs were fabricated with GO and graphene (produced by thermal reduction of GO, see Table S1) based CEs. We found that due to its good electrocatalytic activity and high conductivity, the SGN nanosheets based device showed the best PCE as compared to DSSCs with CEs made using the other heteroatom–doped GN materials (see Figure S1). The successful doping of sulfur atoms onto the GN nanosheets was confirmed using X–ray photoelectron spectroscopy (XPS) (Figure S2a and b). The morphology of the SGN nanosheets examined by scanning electron microscopy (SEM) is depicted in Figure S2c. Although the SGN materials exhibited the highest electrocatalytic activity and lowest charge–transfer resistance (R_{ct}) as compared the other doped GN nanosheets (see Table S2), the PCE of the DSSCs fabricated with this material was

still unsatisfactory. Therefore, further work was needed to improve the performance of this single SGN electrolcatalyst.

Recent studies have demonstrated that FeS_2 is very promising material for DSSC application because of its excellent electrocatalytic activity.[22, 24] In this work, FeS_2 spheres (Figure S2d) were synthesized using a hydrothermal method (see experimental details in the SI).[25] In addition to XPS (see Figure S2e and f for detail), X–ray diffraction (XRD) analysis was used to evaluate the composition of the prepared FeS_2 sample. The majority of the XRD diffraction peaks in **Figure 1**a can be readily indexed to a cubic lattice of pyrite FeS_2 and are in good agreement with the previously published literature.[24, 26] Based on the XRD pattern, we note that some other components such as oxidized Fe (Fe_3O_4) and sulfur were present in the sample. The presence of Fe_3O_4 in the sample was further confirmed by both XPS (Figure S2e and f) and Raman spectroscopy (Figure S3). Notably, recent studies have demonstrated that the Fe_3O_4 possess a good electrocatalytic properties and can be promising candidate for use as CE material in DSSC,[27, 28] while others have reported that sulfur powder can be used to introduce an extra S-doping in GN nanosheets and thus improves the DSSC performance.[29] Based on these studies, we expect that the presence of these components in our sample is beneficial in achieving high efficiency of DSSCs.

The SGN–FeS_2 hybrid electrocatalyst was prepared by mixing and sonicating the previously prepared SGN (Figure S2c) and FeS_2 spheres (Figure S2d) in an ethanol dispersion. The XRD patterns of the samples are illustrated in Figure 1a. The XRD of the SGN sample shows a pronounced broad peak at around $2\theta = 26°$ and a weak peak at $\approx 2\theta = 43.2°$ corresponding to the (002) and (100) diffraction planes, respectively.[15, 30] When analyzing the SGN–FeS_2 (40 wt % FeS_2) hybrid sample, XRD diffraction peaks corresponding to both SGN and FeS_2 throughout the sample were observed. However, the intensity of the diffraction peaks for FeS_2 in the hybrid was very low. This is not unexpected as the 60:40 weight ratio of SGN:FeS_2 corresponds to an atomic ratio on the order of 15:1 meaning the intensity of the X-ray scattering from the carbon material, even with the lower scattering probability from the lighter element, will be much greater than the scattering from the lower amount of FeS_2.

The morphology of the as–prepared hybrid catalyst was examined by SEM. The SEM image in Figure 1b shows that the FeS_2 particles are wrapped by several layers of transparent silk–like SGN nanosheets. It can also be seen from Figure 1c that the FeS_2 particles are well distributed in the SGN nanosheets. Energy dispersive X–ray spectroscopy (EDX) elemental mapping was acquired to further investigate the distribution of different species in this hybrid

electrocatalyst (Figure 1d). EDX elemental mapping confirmed that C, O, Fe and S were uniformly distributed in the SGN–FeS_2 hybrid sample (Figure 1e).

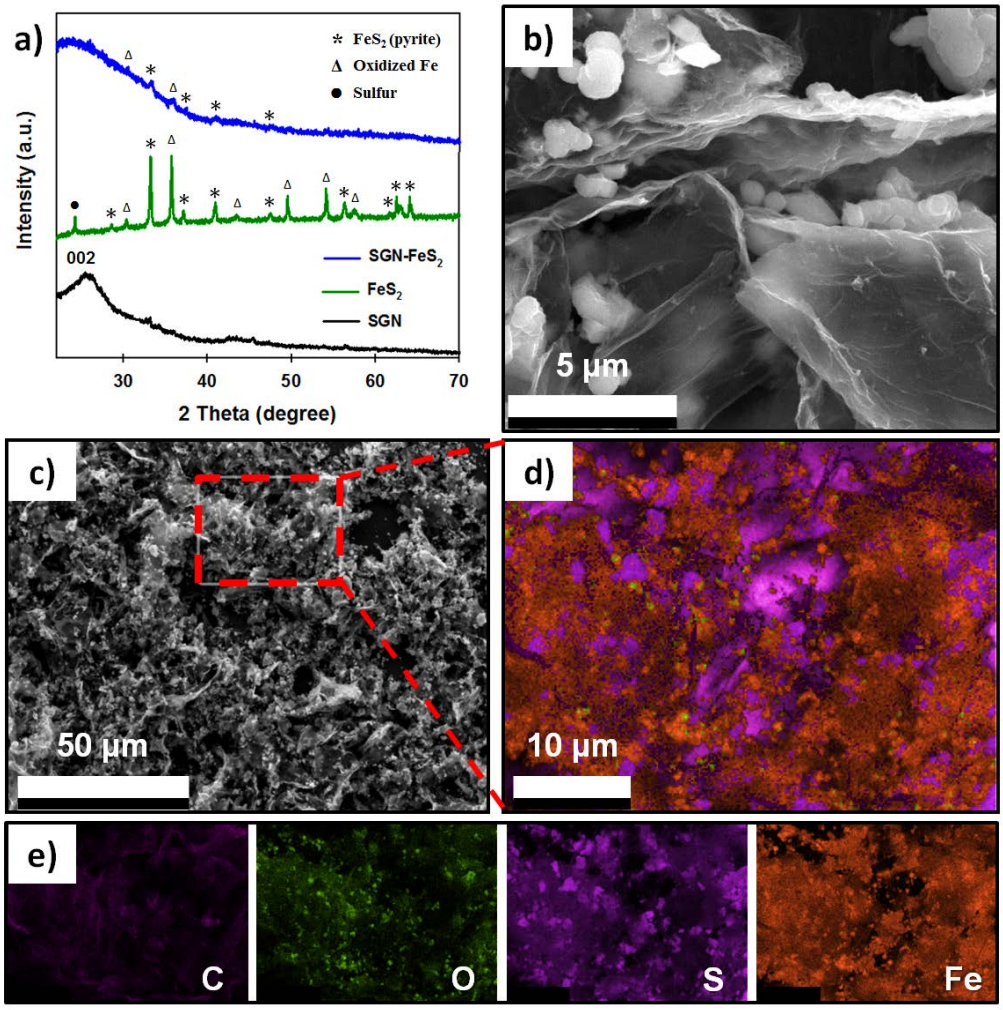

Figure 1. (a) XRD patterns of SGN, FeS_2 and SGN–FeS_2 (40 wt % FeS_2) hybrid samples. (b) High and (c) low resolution SEM image of SGN–FeS_2 hybrid. The red box in the inset is the selected area for EDX elemental mapping. SEM–EDX elemental mapping of (d) overlay image and (e) elemental C, O, S and Fe in the SGN–FeS_2 hybrid sample.

To evaluate the electrocatalytic activity of CEs based on SGN, FeS_2, SGN–FeS_2 hybrid and Pt for the IRR in the DSSC system, cyclic voltammetry (CV) measurements were carried out with a three–electrode system and recorded at the same scan rate of 50 mV s^{-1}. In **Figure 2**a, two pairs of oxidation and reduction peaks (Ox–A/Red–A (left) and Ox–B/Red–B (right)) are clearly observed for all samples, which can be attributed to the oxidation and reduction reactions of I^-/I_3^- and I_3^-/I_2, respectively.[31] Since the main role of the CE in DSSCs is to

catalyze the reduction of I_3^- to I^-, which corresponds to the lower voltage pair of peaks (Ox–A and Red–A) in the CV curves, the characteristics of these peaks were the main focus of our investigation. The peak separation between the anodic and cathodic peaks (E_{pp}) and the peak current density are the main parameters needed to evaluate the electrocatalytic activity of CE materials.[32] In general, an ideal material for IRR – one with the highest electrocatalytic activity – should exhibit the lowest E_{pp} value, while achieving the highest peak current density. As shown in Figure 2a, the SGN–FeS_2 hybrid electrode displayed an E_{pp} value of 0.279 V, which was lower than that of the SGN (0.285 V) and Pt (0.345 V) (**Table 1**). We note that the E_{pp} value of our Pt is consistent with recent studies.[15, 24, 31, 33, 34] Interestingly, the FeS_2 electrode showed an E_{pp} value as low as 0.161 V owing to its known excellent electrocatalytic activity,[22, 24] but its current density from the CV measurement was very low. To determine the mechanism for this low current density value of the FeS_2, we explored the sheet resistance (R_{sheet}) of the thin films based on our samples using a four point probe and their results are summarized in Table 1. We confirm that a very high R_{sheet} ($1.50 \pm 0.09 \times 10^6$ Ω/□) of the FeS_2 is responsible for its low current density. Because of its improved electrical conductivity (see Table 1), the SGN–FeS_2 hybrid electrocatalyst based electrode exhibited a high peak current density. Higher peak current density and lower E_{pp} values (see Figure 2a) suggest that the SGN–FeS_2 hybrid electrocatalyst possess excellent electrochemical activity for the IRR, which is even comparable and/or superior to that of Pt electrode. Moreover, it can be observed from Figure S4 that our SGN–FeS_2 hybrid is electrochemically stable in tri–iodide electrolyte.

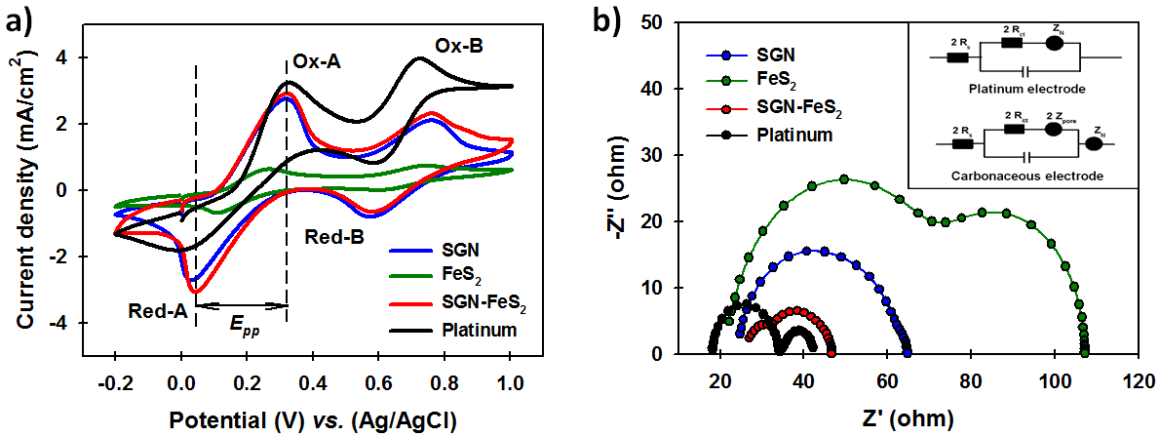

Figure 2. (a) Cyclic voltammograms (CV) of SGN, FeS_2, SGN–FeS_2 hybrid and Pt electrodes in acetonitrile solution containing 10 mM LiI, 1 mM I_2, and 0.1 mM $LiClO_4$ at a scan rate of 50 mV s^{-1}. (b) Nyquist plots of symmetric sandwich cells structure fabricated with different CE materials on FTO electrodes. Inset shows the equivalent circuit diagrams for the control Pt and other electrodes for EIS analysis.

Table 1. Detailed PV parameters of the DSSC devices fabricated based on different CE materials. Average values and the error bars are calculated based on five cells and samples. Parameters of the best cells are highlighted in **bold**. E_{pp}: peak-to-peak voltage separation was calculated from the CV measurements. R_{ct}: charge-transfer resistances were obtained from the EIS analysis by fitting the measured EIS data to a modeled equivalent circuit diagram. R_{sheet}: sheet resistances were measured using a four–point probe technique.

Samples	J_{sc}, (mA cm^{-2})	V_{oc}, (V)	*FF*	PCE, (%)	E_{pp}, (V)	R_{ct}, (Ω)	R_{sheet}, (Ω/□)
SGN	**15.96**; 15.86 ± 0.33	**0.77**; 0.77 ± 0.01	**0.55**; 0.52 ± 0.02	**6.79**; 6.36 ± 0.32	0.285	22.3	2.37 ± 0.54 x 10^3
FeS_2	**15.94**; 15.86 ± 0.37	**0.73**; 0.74 ± 0.01	**0.47**; 0.46 ± 0.02	**5.51**; 5.43 ± 0.09	0.161	39.8	1.50 ± 0.09 x 10^6
SGN–FeS_2	**16.43**; 16.51 ± 0.26	**0.82**; 0.80 ± 0.02	**0.60**; 0.59 ± 0.02	**8.10**; 7.82 ± 0.26	0.279	11.2	4.52 ± 0.15 x 10^3
Platinum	**16.96**; 16.77 ± 0.47	**0.81**; 0.81 ± 0.00	**0.60**; 0.60 ± 0.01	**8.33**; 8.13 ± 0.21	0.345	14.2	–

Electrochemical impedance spectroscopy (EIS) is another important technique to understand the capacity of CE materials to catalyze the IRR in DSSCs. EIS were recorded for the dummy cells consisting of a symmetrical sandwich structure (electrode/(I^-/I_3^- electrolyte)/electrode) with SGN, FeS_2, SGN–FeS_2 hybrid and Pt as electrodes. The Nyquist plots shown in Figure 2b are obtained by fitting the measured EIS data to a modeled equivalent circuit diagram. Typical modeled equivalent circuit diagrams used for Pt and carbon based CEs are illustrated in the inset of Figure 2b. A typical Nyquist plot for CE materials for the IRR consists of two semi-circles.[32, 33, 35] The lower Z´ semicircle is attributed to the R_{ct}, which originates from the interface between CEs and electrolyte; whereas the higher Z´ semicircle is related to ionic diffusion impedance (Z_N) of the redox couples in the electrolyte.[33] Since R_{ct} directly reflects to the performance of the electrocatalyst materials, the measured R_{ct} values of the SGN, FeS_2, SGN–FeS_2 hybrid and Pt cells are listed in Table 1. Due to the combination of excellent conductivity and high catalytic activity, the SGN–FeS_2 hybrid electrocatalyst exhibited the smallest R_{ct} value (11.2 Ω), which was even slightly lower than that of Pt (14.2 Ω) and significantly lower than the values for SGN (22.3 Ω) and FeS_2 (39.8 Ω). The EIS results were in good agreement with the CV results. Overall, the electrochemical characterization (CV and

EIS analysis) clearly indicate that our SGN–FeS_2 electrocatalyst could be used as a promising alternative CE to catalyze the IRR in DSSCs. Therefore, as compared to the Pt CE based devices, we expected to achieve comparable or even higher PV performance of DSSCs using this hybrid electrocatalyst based CEs.

As mentioned earlier, good CE materials should have both high catalytic activity and excellent electrical conductivity to efficiently catalyze the redox reaction and rapidly transfer the electrons in DSSCs.[7] Since our findings from the electrochemical and electrical characterization suggest that the SGN possesses excellent conductivity and FeS_2 has high catalytic activity, the amount (loadings) of SGN or FeS_2 in the hybrid would play an important role for the DSSC performance. There is clearly an optimum concentration of SGN or FeS_2 in the hybrid. Therefore, based on DSSC efficiencies, we optimized the concentration of the SGN or FeS_2 in the hybrid CEs for DSSCs and found that 60 wt% SGN and 40 wt% FeS_2 in the hybrid are the optimum loadings (see **Figure 3**a).

Furthermore, DSSC devices were fabricated using the four electrocatalysts, namely SGN, FeS_2, SGN–FeS_2 and Pt as CE materials. The photocurrent density–voltage (*J*–*V*) characteristics of the DSSCs fabricated with these CEs are illustrated in Figure 3b and the corresponding PV parameters have been summarized in Table 1. The control DSSC fabricated with the conventional Pt CE showed a PCE as high as 8.3% with a short–circuit current (J_{sc}) of 16.96 mA cm^{-2}, open–circuit voltage (V_{oc}) of 0.81 V and fill factor (*FF*) of 0.60. As expected, the PCEs of single SGN–only (6.79%) and FeS_2–only (5.51%) based DSSCs are significantly lower than the conventional Pt CE based devices. The lower PCE of the DSSCs with SGN–only, as compared to the Pt based cells, is mainly due to the lack of electrocatalytic activity, while the poor conductivity of FeS_2 is responsible for its poor PV efficiency. By coupling both excellent conductivity of SGN and high catalytic activity of FeS_2, the cell fabricated with the SGN–FeS_2 hybrid based CE showed a notable enhancement in the PCE as compared to the efficiencies of single SGN–only and FeS_2–only based DSSCs. In particular, the measured J_{sc}, V_{oc}, and *FF* values for this hybrid CE based DSSC were 16.43 mA cm^{-2}, 0.82 V, and 0.60, respectively, and a PCE of 8.1% was achieved. The results of PV performances were in line with our electrochemical characterization (CV and EIS). More importantly, this impressive PCE (8.1%) achieved by the SGN–FeS_2 hybrid electrocatalyst based DSSC was comparable to that (8.3%) of the expensive Pt electrocatalyst based device.

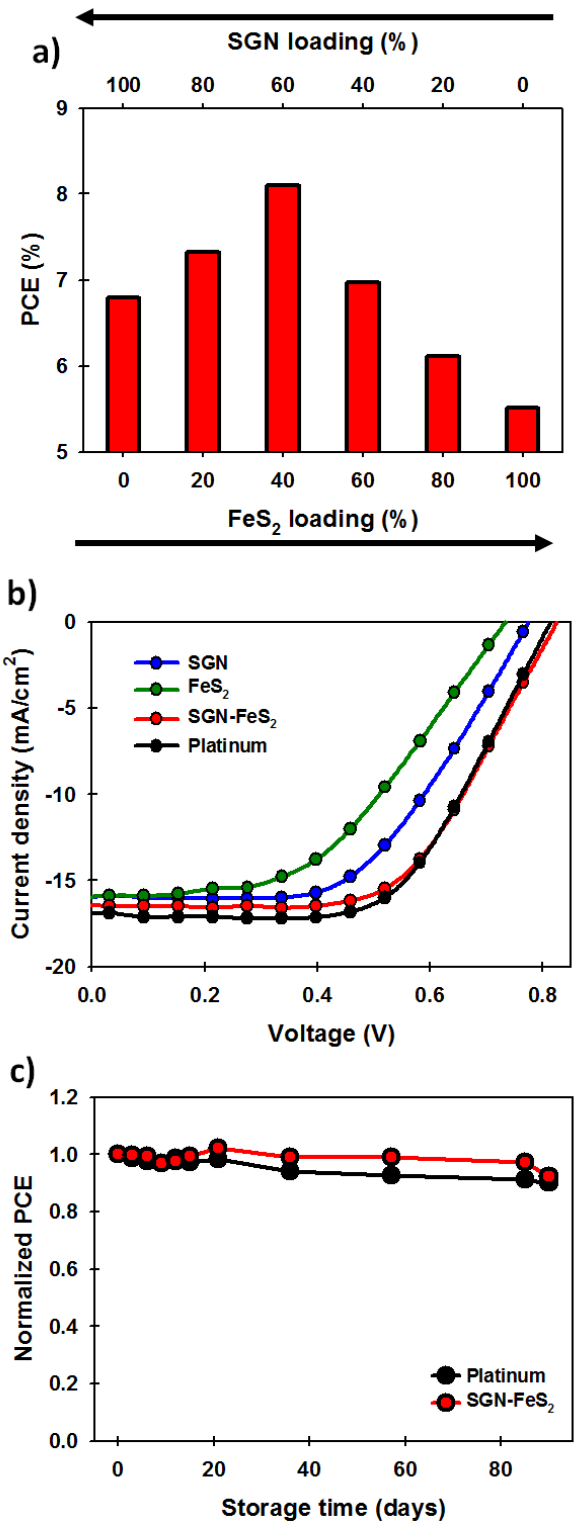

Figure 3. (a) Influence of SGN and FeS_2 loadings in the hybrid on the efficiency of the DSSCs. (b) *J–V* curves of best performing DSSCs fabricated with different CEs. (c) Normalized PCE of DSSCs fabricated with SGN–FeS_2 and Pt as a function of long-term storage time in ambient conditions.

The stability of PV devices is one of the most critical factors for their potential commercialization on an industrial scale. For the storage–stability test, the unencapsulated DSSC devices fabricated with SGN–FeS_2 and Pt CEs were kept in ambient conditions for 90 days. Normalized PCEs of these two devices are plotted in Figure 3c. It can be seen from Figure 3c that the SGN–FeS_2 hybrid CE based DSSC showed excellent storage–stability (more than 90% of initial PCE after 90 days of storage was retained), comparable to the stability of the Pt-based cell. This excellent stability of our SGN–FeS_2 hybrid based DSSC confirms the good electrochemical stability explored using CV measurements (see Figure S4) of this electrocatalyst.

In summary, in this work, a series of heteroatom (I, P, B, N, S)–doped graphene materials have been prepared and employed as CE materials to catalyze the IRR in DSSCs. We found based on the electrochemical characterization and PV analysis that the elemental S–doping on graphene is the most effective in improving the electrocatalytic activity among other types of doping atoms. Of particular note, however, is the combination of this material with FeS_2 yielded a CE material whose electrocatalytic activity and electrochemical stability is comparable to that of the standard Pt-based CE. The combination of high electrocatalytic activity, good electrical conductivity, outstanding electrochemical stability and impressive device performance of the SGN–FeS_2 hybrid electrocatalyst makes this material an ideal candidate for highly efficient and stable DSSCs.

Supporting Information
Supporting Information is available from the Wiley Online Library or from the author.

Acknowledgements
The support of the Australian Research Council Discovery Program (DP130101714, DP150101354 and DP160101301) is gratefully acknowledged. Munkhbayar Batmunkh acknowledges International Postgraduate Research Scholarship (IPRS) and Australian Postgraduate Award (APA) for their financial support during his study in Australia.We acknowledge the use of South Australian nodes of the Australian Microscopy & Microanalysis Research Facility (AMMRF) and the Australian National Fabrication Facility (ANFF) at Flinders University. The authors would also like to thank Jade Taylor and Yanting Yin of School of Chemical and Physical Sciences at Flinders University for their help with the XPS analysis.

Received: ((will be filled in by the editorial staff))
Revised: ((will be filled in by the editorial staff))
Published online: ((will be filled in by the editorial staff))

References

[1] S. Zhang, X. Yang, Y. Numata, L. Han, *Energy Environ. Sci.* **2013**, *6*, 1443.
[2] M. Batmunkh, M. J. Biggs, J. G. Shapter, *Adv. Sci.* **2015**, *2*, 1400025.
[3] M. Ye, X. Wen, M. Wang, J. Iocozzia, N. Zhang, C. Lin, Z. Lin, *Mater. Today.* **2015**, *18*, 155.
[4] S. Hwang, M. Batmunkh, M. J. Nine, H. Chung, H. Jeong, *ChemPhysChem.* **2015**, *16*, 53.
[5] J. Briscoe, S. Dunn, *Adv. Mater.* **2016**, *28*, 3802.
[6] M. Janani, P. Srikrishnarka, S. V. Nair, A. S. Nair, *J. Mater. Chem. A.* **2015**, *3*, 17914.
[7] H. Wang, Y. H. Hu, *Energy Environ. Sci.* **2012**, *5*, 8182.
[8] S. Thomas, T. G. Deepak, G. S. Anjusree, T. A. Arun, S. V. Nair, A. S. Nair, *J. Mater. Chem. A.* **2014**, *2*, 4474.
[9] M. Batmunkh, M. J. Biggs, J. G. Shapter, *Small.* **2015**, *11*, 2963.
[10] S. Yun, A. Hagfeldt, T. Ma, *Adv. Mater.* **2014**, *26*, 6210.
[11] J. Zhang, M. Yu, S. Li, Y. Meng, X. Wu, J. Liu, *J. Power Sources.* **2016**, *334*, 44.
[12] H. Wang, K. Sun, F. Tao, D. J. Stacchiola, Y. H. Hu, *Angew. Chem. Int. Ed.* **2013**, *52*, 9210.
[13] B. Munkhbayar, M. J. Nine, J. Jeoun, M. Ji, H. Jeong, H. Chung, *J. Power Sources* **2013**, *230*, 207.
[14] Q. Luo, F. Hao, S. Wang, H. Shen, L. Zhao, J. Li, M. Grätzel, H. Lin, *J. Phys. Chem. C.* **2014**, *118*, 17010.
[15] X. Meng, C. Yu, X. Song, Y. Liu, S. Liang, Z. Liu, C. Hao, J. Qiu, *Adv. Energy Mater.* **2015**, *5*, 1500180.
[16] H. Fang, C. Yu, T. Ma, J. Qiu, *Chem. Commun.* **2014**, *50*, 3328.
[17] Z. Wang, P. Li, Y. Chen, J. He, J. Liu, W. Zhang, Y. Li, *J. Power Sources.* **2014**, *263*, 246.
[18] A. G. Kannan, J. Zhao, S. G. Jo, Y. S. Kang, D.-W. Kim, *J. Mater. Chem. A.* **2014**, *2*, 12232.
[19] D. Yu, E. Nagelli, F. Du, L. Dai, *J. Phys. Chem. Lett.* **2010**, *1*, 2165.
[20] Z. Yang, Z. Yao, G. Li, G. Fang, H. Nie, Z. Liu, X. Zhou, X. a. Chen, S. Huang, *ACS Nano.* **2012**, *6*, 205.
[21] Y. Jiao, Y. Zheng, M. Jaroniec, S. Z. Qiao, *J. Am. Chem. Soc.* **2014**, *136*, 4394.
[22] Y.-C. Wang, D.-Y. Wang, Y.-T. Jiang, H.-A. Chen, C.-C. Chen, K.-C. Ho, H.-L. Chou, C.-W. Chen, *Angew. Chem. Int. Ed.* **2013**, *52*, 6694.
[23] Q.-H. Huang, T. Ling, S.-Z. Qiao, X.-W. Du, *J. Mater. Chem. A.* **2013**, *1*, 11828.
[24] S. Shukla, N. H. Loc, P. P. Boix, T. M. Koh, R. R. Prabhakar, H. K. Mulmudi, J. Zhang, S. Chen, C. F. Ng, C. H. A. Huan, N. Mathews, T. Sritharan, Q. Xiong, *ACS Nano.* **2014**, *8*, 10597.
[25] M. Zhang, B. Chen, H. Tang, G. Tang, C. Li, L. Chen, H. Zhang, Q. Zhang, *RSC Adv.* **2015**, *5*, 1417.
[26] H. Xue, D. Y. W. Yu, J. Qing, X. Yang, J. Xu, Z. Li, M. Sun, W. Kang, Y. Tang, C.-S. Lee, *J. Mater. Chem. A.* **2015**, *3*, 7945.
[27] L. Wang, Y. Shi, H. Zhang, X. Bai, Y. Wang, T. Ma, *J. Mater. Chem. A* **2014**, *2*, 15279.
[28] H. Zhou, J. Yin, Z. Nie, Z. Yang, D. Li, J. Wang, X. Liu, C. Jin, X. Zhang, T. Ma, *J. Mater. Chem. A* **2016**, *4*, 67.
[29] X. Meng, C. Yu, X. Song, Z. Liu, B. Lu, C. Hao, J. Qiu, *J. Mater. Chem. A* **2017**, *5*, 2280.

[30] L. Mei, H. Zhao, B. Lu, *Adv. Sci.* **2015**, *2*, 1500116.
[31] A. Shrestha, M. Batmunkh, C. J. Shearer, Y. Yin, G. G. Andersson, J. G. Shapter, S. Qiao, S. Dai, *Adv. Energy Mater* **2017**, *7*, 1602276.
[32] X. Cui, J. Xiao, Y. Wu, P. Du, R. Si, H. Yang, H. Tian, J. Li, W.-H. Zhang, D. Deng, X. Bao, *Angew. Chem. Int. Ed.* **2016**, *55*, 6708.
[33] E. Bi, H. Chen, X. Yang, W. Peng, M. Gratzel, L. Han, *Energy Environ. Sci.* **2014**, *7*, 2637.
[34] Y. Duan, Q. Tang, J. Liu, B. He, L. Yu, *Angew. Chem. Int. Ed.* **2014**, *53*, 14569.
[35] Y. Xue, J. Liu, H. Chen, R. Wang, D. Li, J. Qu, L. Dai, *Angew. Chem. Int. Ed.* **2012**, *51*, 12124.

The combination of high electrocatalytic activity, excellent electrical conductivity, outstanding electrochemical stability and impressive device performance of the sulfur-doped graphene nanosheets with FeS_2 spheres based hybrid electrocatalyst makes this material an ideal candidate for highly efficient and stable DSSCs.

Keyword: counter electrode, dye-sensitized solar cells, doping, graphene, iron disulfide

Munkhbayar Batmunkh, Aabhash Shrestha, Gao Guo, Leping Yu, Jing Zhao, Mark. J. Biggs, Cameron J. Shearer and Joseph G. Shapter*

Sulfur–Doped Graphene with Iron Pyrite (FeS_2) as an Efficient and Stable Electrocatalyst for Iodine Reduction Reaction in Dye–sensitized Solar Cells

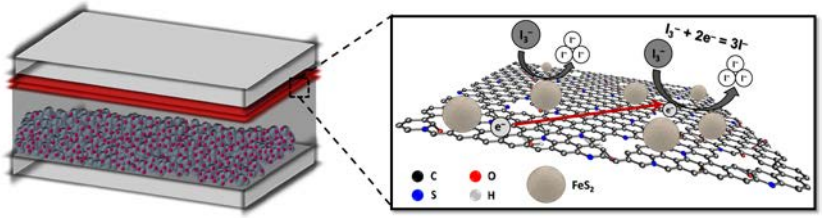

Supporting Information

Sulfur–Doped Graphene with Iron Pyrite (FeS_2) as an Efficient and Stable Electrocatalyst for the Iodine Reduction Reaction in Dye–sensitized Solar Cells

*Munkhbayar Batmunkh, Aabhash Shrestha, Gao Guo, Leping Yu, Jing Zhao, Mark. J. Biggs, Cameron J. Shearer and Joseph G. Shapter**

Munkhbayar Batmunkh, Dr. Aabhash Shrestha, Prof. Mark J. Biggs
School of Chemical Engineering, The University of Adelaide, Adelaide, South Australia 5005, Australia

Munkhbayar Batmunkh, Leping Yu, Dr. Jing Zhao, Dr. Cameron J. Shearer, Prof. Joseph G. Shapter
Centre for Nanoscale Science and Technology, School of Chemical and Physical Sciences, Flinders University, Bedford Park, Adelaide, South Australia 5042, Australia
E-mail: joe.shapter@flinders.edu.au

Prof. Gao Guo
Institute of Nano Biomedicine and Engineering, Shanghai Engineering Research Center for Intelligent Diagnosis and Treatment Instrument, Department of Instrument Science and Engineering, School of Electronic Information and Electrical Engineering, Shanghai Jiao Tong University, 800 Dongchuan Road, Shanghai 200240, P. R. China

Prof. Mark J. Biggs
School of Science, Loughborough University, Loughborough, Leicestershire, LE11 3TU, UK

Experimental Section

Materials:

Unless otherwise specified, all chemicals used in this work were obtained from Sigma–Aldrich. Sodium hydroxide (NaOH) (purity >98%) and sulfur (S) (purity >98%) powders were purchased from Chem–Supply Pty Ltd. Ruthenizer 535–bisTBA (N719 dye), iodide/tri–iodide electrolyte (Iodolyte Z–50), DuPont Surlyn® (Meltonix 1170–60) and Platinum (Pt) catalyst (Platisol T) were purchased from Solaronix, Switzerland. A fluorine–doped tin oxide (FTO) coated glass electrodes with a sheet resistance (R_s) of ~8 Ω/□ (TEC8), transparent TiO_2 paste (18NR–T), reflector TiO_2 paste (WER2–O) were purchased from Dyesol, Australia.

Preparation of graphene oxide (GO):

Graphene oxide (GO) was prepared *via* the oxidation and exfoliation of natural graphite according to an improved Hummers method reported by Marcano et al.[1] In brief, a 9:1 (*v:v*) mixture of sulfuric acid (95–98% H_2SO_4) and phosphoric acid (85% H_3PO_4) (240:27 mL) was kept in the cold (3–5^{o}C) until it was added to a mixture of graphite flakes (2 g) and potassium permanganate (99% $KMnO_4$) (12 g). The oxidation process of graphite was carried out by stirring the mixture at ~50 ^{o}C for 12 h. Then, the reaction was cooled down to room temperature and poured onto ice (300 mL) with 30% hydrogen peroxide (H_2O_2) (2 mL). The mixture was then washed with distilled (DI) water, 30% hydrochloric acid (HCl) and ethanol (x 2 times). For each sequential wash, the product was centrifuged at 4400 rpm for 3 h and the supernatant decanted away. The light brown sample obtained was dispersed and exfoliated in an aqueous solution, and then freeze–dried to obtain GO powder.

Preparation of heteroatom–doped graphene:

Different heteroatom (I, P, B, N, S)–doped graphene were prepared by the carbonization of the mixture of GO and dopant precursor in a programmable tube furnace under N_2 atmosphere using a previously established method.[2] Typically, 100 mg of GO and 500 mg of precursor (see Table S1 for the types of dopant precursors) were ground in a ceramic mortar to form the mixture powder of GO and precursor. The mixture was then poured into a crucible and carbonized at 900 ^{o}C for 3 h with a heating rate of 5 ^{o}C min^{-1}. The calcination process includes five steps: 1) purge the tube furnace with N_2 gas at room temperature for 30 min, 2)

increase the temperature to 120 ^{o}C, 3) Hold at 120 ^{o}C for 2 hr to remove moisture in the GO, 4) Increase the temperature to 900 ^{o}C, 5) Hold at 900 ^{o}C for 3 hrs, followed by cooling down to room temperature. The heating ramp for all heating and/or calcining processes was 5 ^{o}C min^{-1}.

Preparation of FeS_2 particles:

The FeS_2 partciles were synthesized using a hydrothermal method according to a previously reported method with slight modifications.[3] In a typical experiment, Polyvinylpyrrolidone (PVP) and poly (ethylene glycol) (PEG–6000) (1.5 : 1 weight ratio) were dissolved in 10 mL DI water and stirred for 15 min to obtain a completely dissolved transparent solution. 2.2 g $FeCl_2 \cdot 4H_2O$ was then added into the above solution, followed by gradual addition of 10 mL NaOH solution (0.5 M) with stirring. Then, 0.2 g S powder was also added into the solution, followed by stirring and sonication three times. After obtaining a well dissolved precursor solution, the sample was transferred into a hydrothermal reactor and heated to 200 ^{o}C for 12 h. After the reaction, the sample obtained was filtered, washed with DI water and ethanol, and dried for further use.

Preparation of pastes and counter electrodes:

Viscous pastes based on different electrocatalysts including GO, GN, IGN, PGN, BGN, NGN, SGN, FeS_2 and SGN–FeS_2 hybrid were prepared according to the established procedures described in the literature without any modification.[4] Ethyl cellulose was used as an adhesive binder for the pastes. For the preparation of hybrid pastes, the concentrations of SGN or FeS_2 in the hybrid were varied from 0 to 100 wt% with an interval of 20 wt% (*e.g.* weight ratio of 100% : 0%, 80% : 20%, 60% : 40%, 40% : 60%, 20% : 80%, and 0% : 100%,). The as–prepared pastes were sonicated for 5 min before use and then coated onto the cleaned FTO electrodes via a doctor blade technique. The FTO glass was cleaned with a detergent followed by washing with Milli–Q water, acetone and ethanol under ultrasonication for 10 min each before use. After the paste deposition onto the FTO electrodes, the films were dried in an oven at 90 ^{o}C for 5–10 min and annealed at 420 ^{o}C for 30 min under the protection of Argon gas. In the meantime, for comparison, Pt CEs were prepared by coating Pt precursor onto FTO substrates using a brush–painting method, followed by platinizing at 450 ^{o}C for 20 min. Finally, the prepared counter electrodes (CEs) were cooled to room temperature.

Device fabrication:

The N719 dye–sensitized solar cell devices were fabricated as reported elsewhere.[5] Briefly, the cleaned FTO glass electrodes were first immersed into a 40 mM aqueous $TiCl_4$ solution at 70 ^oC for 30 min, and rinsed with water and ethanol. Then, ~10 μm thick transparent TiO_2 layers (Dyesol 18NR–T, 20 nm in diameter) were deposited on the FTO electrodes by a doctor blading technique. The transparent TiO_2 films were gradually heated under an air flow at 125 ^oC for 5 min, 325 ^oC for 5 min, at 375 ^oC for 15 min and at 450 ^oC for 30 min, followed by cooling to room temperature. Then, ~6 μm thick reflector TiO_2 layers (Dyesol WER2–O, 150–250 nm in diameter) were coated on the transparent TiO_2 layers. The photoelectrodes coated with transparent and reflector TiO_2 layers were sintered at 500 ^oC for 1 h. After sintering, the photoelectrodes were immersed in aqueous $TiCl_4$ (40 mM) solution at 70 ^oC for 30 min, followed by final annealing at 500 ^oC for 1 h. After cooling to ~50 ^oC, the prepared TiO_2 films were immersed into 0.5 mM N719 dye in an ethanol solution for 20 h at room temperature. The dye adsorbed photoelectrodes and previously prepared CEs were assembled into a sealed sandwich–type cell, with a 60 μm thick hot–melt sealing Surlyn between each layer. The electrolyte solution, Iodolyte Z–50 (Solaronix), was introduced into the cell via a vacuum–filling method through an injection hole on the CE side. Finally, the hole was sealed with scotch tape.

Characterization and measurements:

Scanning electron microscopy (SEM) images were obtained using an Inspect F50 SEM (FEI) with accelerating voltage of 20 kV. Energy dispersive X–ray spectroscopy (EDX) elemental mapping analysis was completed on the same system with a Team EDS Octane Pro (EDAX) attachment. X–ray diffraction (XRD) patterns were carried out on a powder X–ray diffractometer at 40 kV and 15 mA in the range of 2θ = 10–80° using Cu Kα radiation (Model Miniflex 600, Rigaku, Japan). X–ray photoelectron spectroscopy (XPS) using a Leybold Heraeus LHS–10 with a SPECS XR–50 dual anode source operating at 250W was carried out at binding energy ranging from 0 eV to 1200 eV. The Mg–Kα source, which has energy of 1253.6 eV, was used for the XPS analysis. Curve fitting of the XPS spectra was done using peak fitting software "CASA XPS". High resolution XPS spectra were collected with a step size of 0.1 eV and the presented spectra are an average of 5 collections. The XPS spectra were referenced to the carbon 1s peak at 284.5 eV.

Both cyclic voltammetry (CV) and electrochemical impedance spectroscopy (EIS) measurements were performed using an electrochemical analysis workstation (Autolab Nova Potentiostat). The CV was carried out in a three electrode system with different CE materials as the working electrode, a platinum wire as the counter electrode, and Ag/Ag^{+} electrode as the reference electrode, at a scan rate of 50 mV s^{-1}. For the preparation of the working electrode, 15 µL ink of each sample was dropped on the mirror polished glassy carbon electrodes. The electrodes were dipped in an anhydrous acetonitrile solution containing 10 mM LiI, 1 mM I_2, and 0.1 mM $LiClO_4$. EIS measurements were carried out by scanning the symmetric cells with the structure of CE/electrolyte/CE. The resultant EIS spectra were analyzed by means of the Z–view software.

Sheet resistance measurements were performed on the SGN, FeS_2 and SGN–FeS_2 hybrid coated microscope slides using a four point probe technique (KeithLink Technology Co., Ltd. Taiwan).

The photocurrent–voltage (*J*–*V*) characteristics were analyzed using a Keithley 2400 SMU instrument and recorded using a custom LabView Virtual Instrument program. A standard silicon test cell with NIST-traceable certification was used to calibrate the power density as 100 mW cm^{-2} at the sample plane of the collimated a 150W xenon–arc light source (Newport), which was passed through an AM 1.5G filter. The active area of the fabricated devices was 0.19 cm^2.

Table S1. Experimental conditions and parameters for the preparation of different heteroatom doped graphene electrocatalysts. For the preparation of all samples, graphene oxide ((GO), prepared from natural graphite using improved synthesis method) was used as a starting material. The weight ratio of GO : precursor was 1 : 5 for all samples.

Samples	***Doping Precursor***	***Annealing Temperature***	***Annealing Time***	***Gas***
Graphene Oxide	-	-	-	-
Graphene	-	900^{o}C	3 h	N_2
I-doped Graphene	Iodine (I_2)	900^{o}C	3 h	N_2
P-doped Graphene	Triphenylphosphine ($C_{18}H_{15}P$)	900^{o}C	3 h	N_2
B-doped Graphene	Boric Acid (H_3BO_3)	900^{o}C	3 h	N_2
N-doped Graphene	Melamine ($C_3H_6N_6$)	900^{o}C	3 h	N_2
S-doped Graphene	Diphenylsulfide ($C_{12}H_{10}S_2$)	900^{o}C	3 h	N_2

Five individual nonmetallic elements (I, P, B, N, S) were introduced onto GN nanosheets to obtain single atom-doped GN materials. These materials (IGN, PGN, BGN, NGN and SGN) were prepared from GO by using different types of precursors under the same experimental conditions (see Table S1). GO was prepared via the oxidation of natural graphite according to an improved Hummers method.[1]

The prepared heteroatom–doped GN materials were used to fabricate DSSC devices. It should be noted that the thickness of mesoporous TiO_2 layer in these DSSCs was ~9–10 µm achieved by using 1 layer of 3M scotch tape. This thin TiO_2 layer resulted in slightly lower short-circuit current (J_{sc}) values (see Figure S1 and Table S2) and was intentionally used in order to compare these various types of doped graphene CEs for DSSCs.

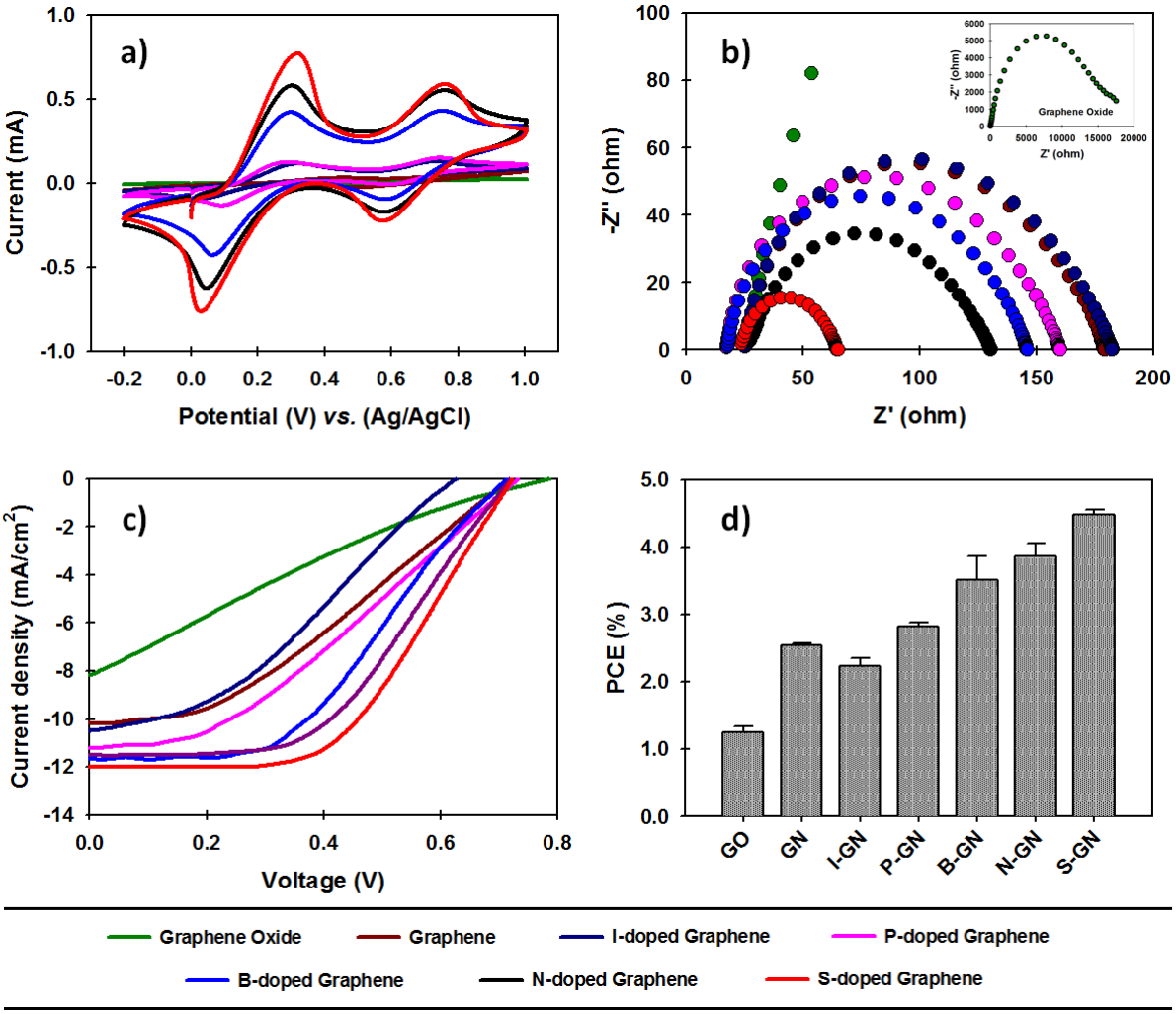

Figure S1. (a) Cyclic voltammograms (CV) and (b) electrochemical impedance spectra (EIS) of various heteroatom doped graphene (GN) electrodes for IRR. Inset shows the EIS of graphene oxide (GO). (c) Photocurrent-voltage (*J*–*V*) curves and (d) PCE comparison of DSSC devices fabricated with different heteroatom doped graphene based counter electrodes (CEs). Note: These devices were fabricated based on only ~9–10 μm TiO_2 mesoporous layer (without light scattering layer).

Table S2. Photovoltaic (PV) parameters of different heteroatom doped graphene CEs based DSSCs. Note: These devices were fabricated based on only ~9–10 μm TiO_2 mesoporous layer (without light scattering layer). The average values and standard deviations are calculated based on at least three devices. Parameters of the best cells are highlighted in bold. The charge transfer resistances (R_{ct}) were calculated by fitting the electrochemical impedance spectra (EIS) of dummy cells with a symmetric sandwich-like structure fabricated with different CE materials.

Samples	J_{sc} (mA cm^{-2})	V_{oc} (V)	*FF*	*PCE (%)*	R_{ct} (Ω)
Graphene Oxide	**8.158**; 8.49 ± 0.76	**0.786**; 0.76 ± 0.03	**0.21**; 0.19 ± 0.02	**1.34**; 1.25 ± 0.09	3100
Graphene	**10.154**; 9.96 ± 0.28	**0.719**; 0.73 ± 0.02	**0.35**; 0.35 ± 0.00	**2.58**; 2.54 ± 0.04	92.4
I-doped Graphene	**10.487**; 10.79 ± 0.43	**0.629**; 0.61 ± 0.02	**0.35**; 0.34 ± 0.01	**2.32**; 2.24 ± 0.11	94.2
P-doped Graphene	**11.168**; 11.06 ± 0.11	**0.733**; 0.73 ± 0.01	**0.35**; 0.35 ± 0.00	**2.88**; 2.83 ± 0.05	83.3
B-doped Graphene	**11.622**; 11.32 ± 0.42	**0.714**; 0.71 ± 0.01	**0.45**; 0.44 ± 0.02	**3.75**; 3.51 ± 0.35	70.9
N-doped Graphene	**11.493**; 11.55 ± 0.07	**0.721**; 0.71 ± 0.01	**0.49**; 0.47 ± 0.02	**4.09**; 3.87 ± 0.19	44.0
S-doped Graphene	**11.970**; 11.92 ± 0.09	**0.723**; 0.72 ± 0.01	**0.53**; 0.53 ± 0.01	**4.60**; 4.49 ± 0.07	22.3

High-resolution X-ray photoelectron spectroscopy (XPS) spectra for the C 1s and S 2p regions of the SGN sample are shown in Figure S2a and b, respectively. The C 1s peak for the SGN material was observed at ~284.5 eV, which is consistent with graphene sp^2 carbon in the samples.[6, 7] Moreover, there are some minor shoulder contributions to the XPS signals at binding energies of 285.0–288.0 eV, which can be assigned to sulfur- and/or oxygen-bound carbon atoms on the surface of SGN nanosheets.[8] Another broad peak at binding energies of 287.0–290.0 eV is assigned to the C=O and O–C=O chemical environments, which is in agreement with previous literature.[9] The broad signals at 290.0–292.0 eV correspond to the π–π* shake-up peak. The main peaks in the S 2p for the XPS spectra of SGN material are at binding energies of around 163.7 eV and 164.9 eV can be attributed to the spin-orbit splitting of S atoms doped onto the graphene layers, *e.g.* S dominated in the graphene via the formation of the sulfide bridges. This result is in very good agreement with the literature.[10, 11]

The Fe 2p and S 2p spectra are illustrated in Figure S2e and f, respectively. In Figure 2e, there are two predominant peaks at binding energies of around 707 eV (Fe $2p_{3/2}$) and 720.0 eV (Fe $2p_{1/2}$), which are consistent with the binding energies of Fe in the Fe(II)–S bond.[12] The binding energy values at around 711.1 and 724.5 eV can be assigned to the $2p_{3/2}$ and $2p_{1/2}$, respectively in Fe_3O_4. Furthermore, in Figure S2f, the $2p_{3/2}$ and S $2p_{1/2}$ peaks at around 163 eV and 164.2 eV, respectively are also consistent with the sulfur binding energy in the FeS_2.[13]

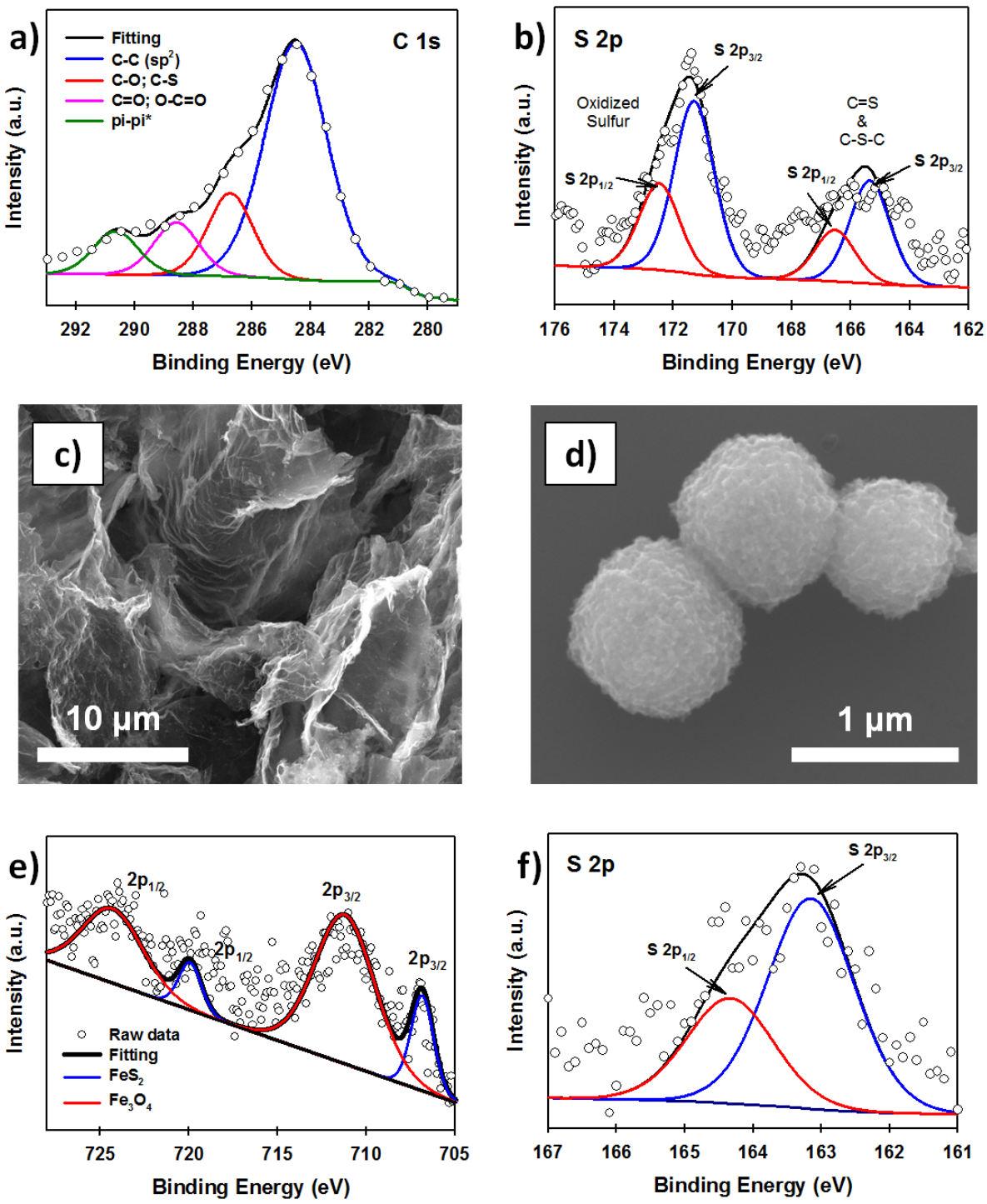

Figure S2. (a) C 1s and (b) S 2p XPS spectra of SGN sample. SEM image of (c) SGN nanosheets and (d) FeS_2 spheres. (e) Fe 2p and (f) S 2p XPS spectra of the prepared sample.

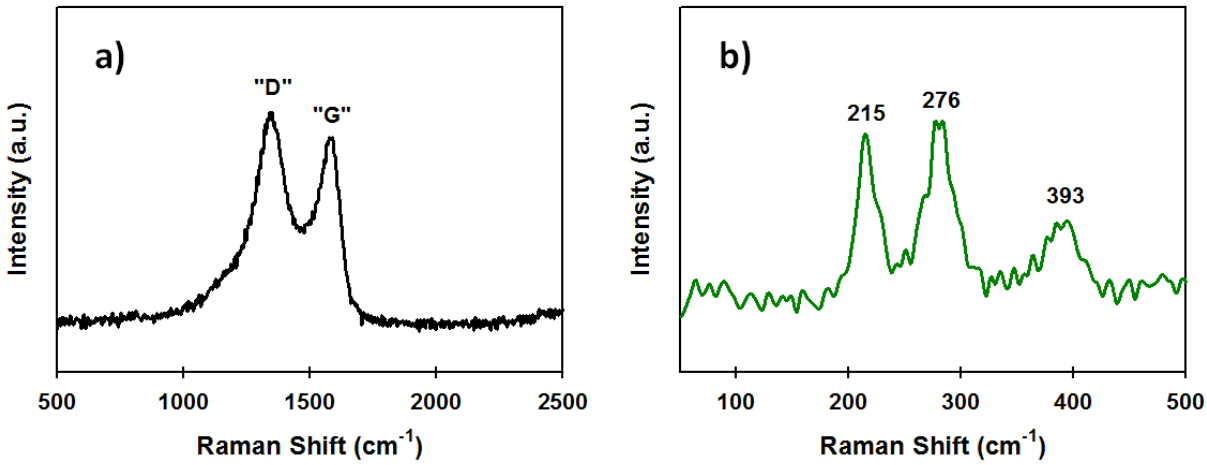

Figure S3. Raman spectrum of (a) SGN and (b) FeS_2 sample.

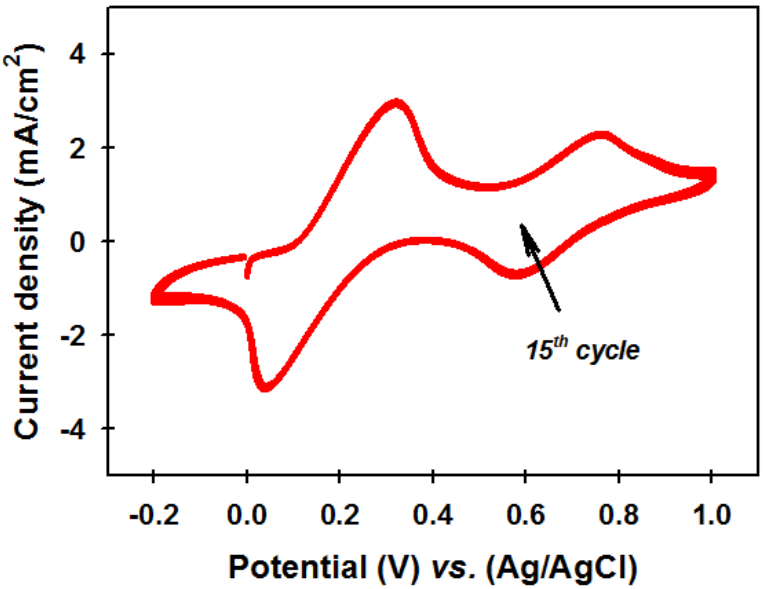

Figure S4. Electrochemical stability of SGN–FeS_2 hybrid electrocatalyst tested by measuring CV for 15 cycles.

References

[1] D. C. Marcano, D. V. Kosynkin, J. M. Berlin, A. Sinitskii, Z. Sun, A. Slesarev, L. B. Alemany, W. Lu, J. M. Tour, *ACS Nano.* **2010**, *4*, 4806.

[2] Y. Jiao, Y. Zheng, M. Jaroniec, S. Z. Qiao, *J. Am. Chem. Soc.* **2014**, *136*, 4394.

[3] M. Zhang, B. Chen, H. Tang, G. Tang, C. Li, L. Chen, H. Zhang, Q. Zhang, *RSC Adv.* **2015**, *5*, 1417.

[4] J. D. Roy-Mayhew, G. Boschloo, A. Hagfeldt, I. A. Aksay, *ACS Appl. Mater. Interfaces.* **2012**, 4, 2794.
[5] M. Batmunkh, M. Dadkhah, C. J. Shearer, M. J. Biggs, J. G. Shapter, *Energy Technol.* **2016**, *4*, 959.
[6] W. Li, Z. Zhang, Y. Tang, H. Bian, T.-W. Ng, W. Zhang, C.-S. Lee, *Adv. Sci.* **2016**, *3*, 1500276.
[7] S. Chen, J. Duan, J. Ran, S.-Z. Qiao, *Adv. Sci.* **2015**, *2*, 1400015.
[8] Q. Xu, P. Pu, J. Zhao, C. Dong, C. Gao, Y. Chen, J. Chen, Y. Liu, H. Zhou, *J. Mater. Chem. A.* **2015**, *3*, 542.
[9] J. Balamurugan, T. D. Thanh, N. H. Kim, J. H. Lee, *Adv. Mater. Interf.* **2016**, *3*, 1500348.
[10] J. Wang, R. Ma, Z. Zhou, G. Liu, Q. Liu, *Sci. Rep.* **2015**, *5*, 9304.
[11] Q. Luo, F. Hao, S. Wang, H. Shen, L. Zhao, J. Li, M. Grätzel, H. Lin, *J. Phys. Chem. C.* **2014**, *118*, 17010.
[12] P. Bonnissel-Gissinger, M. Alnot, J.-J. Ehrhardt, P. Behra, *Environ. Sci. Technol*. **1998**, *32*, 2839.
[13] X. Wen, X. Wei, L. Yang, P. K. Shen, *J. Mater. Chem. A.* **2015**, *3*, 2090.